Check for updates

Journal of Magnetic Resonance Imaging

GUIDELINES OPEN ACCESS

Construction of Phantoms for MR Electrical Properties Tomography (From Structure to Composition): A Guideline From the ISMRM Electro-Magnetic Tissue Properties Study Group

Ilias I. Giannakopoulos[1] | Alessandro Arduino[2] | Cornelis A. T. van den Berg[3] | Zhongzheng He[4] | Kyu-Jin Jung[5] | Dong-Hyun Kim[5] | Riccardo Lattanzi[1] | Jessica A. Martinez[6,7] | Thierry Meerbothe[3] | Freddy Odille[4,8] | Adriano Troia[2] | Luca Zilberti[2] | Stefano Mandija[3]

[1]Department of Radiology, Bernard and Irene Schwartz Center for Biomedical Imaging and Center for Advanced Imaging Innovation and Research (CAI^{2}R), New York University Grossman School of Medicine, New York, New York, USA | [2]Istituto Nazionale di Ricerca Metrologica, Torino, Italy | [3]Computational Imaging Group for MR Therapy and Diagnostic, Department of Radiotherapy, University Medical Center Utrecht, Utrecht, the Netherlands | [4]IADI U1254, INSERM and Université de Lorraine, Nancy, France | [5]Department of Electrical and Electronic Engineering, Yonsei University, Seoul, Republic of Korea | [6]National Institute of Standards and Technology (NIST), Boulder, Colorado, USA | [7]Department of Physics, University of Colorado Boulder, Boulder, Colorado, USA | [8]CIC-IT 1433, Inserm, Université de Lorraine and CHRU Nancy, Nancy, France

Correspondence: Ilias I. Giannakopoulos (iliasgiannako@gmail.com)

Received: 10 February 2025 | **Revised:** 21 April 2025 | **Accepted:** 10 July 2025

Funding: This work was supported by National Institutes of Health (K99 EB035163, P41 EB017183); NIST-PREP (70NANB18H006); NWO-VENI (18078) and by the European Partnership on Metrology (24DIT01 APULEIO).

Keywords: electrical tissue properties | phantom fabrication | phantom guidelines

MR-based Electrical Properties (EPs) Tomography (MR-EPT) denotes non-invasive electrical conductivity (σ_e) and permittivity (ε_r) mapping methods using MR measurements. The lack of standardized tissue-mimicking phantoms hinders reproducibility studies and method comparisons. For example, the NIST/ISMRM MRI system phantom has contributed significantly to standardization efforts in relaxometry, underscoring the importance of having similar benchmarks for MR-EPT. The guidelines presented herein outline the importance of MR-EPT phantom design and construction, focusing on structure, composition, and reliability.

1 | Phantom Structure

The structure should mimic the shape and size of the anatomy of interest. For example, the head can be modeled using a simple spherical geometry or with anatomically realistic designs such as the one presented in [1]. The abdomen can be represented using large elliptic cylindrical phantoms or specialized holders that conform to human anatomy and are commonly used for training purposes [2, 3]. This allows for testing compatibility with standard receive coils and allows the use of established methods to mitigate B_0 inhomogeneity artifacts and spurious phase contributions. Phantoms that are too small to sufficiently load the coil could detune the coil elements or couple opposite receivers. Moreover, phantoms with translational symmetry along the longitudinal axis and significantly larger geometry in the Frankfort horizontal orientation (B_0 direction) than the anterior-to-posterior and right-to-left (e.g., cylinders with length $\geq 4\times$ radius) orientations are ideal for 2D MR-EPT methods since the derivatives along z of B_1 in the midplane of a birdcage coil are approximately null. However, they do not provide a good validity test for human anatomies.

Ilias I. Giannakopoulos and Alessandro Arduino contributed equally to this work.

This is an open access article under the terms of the Creative Commons Attribution License, which permits use, distribution and reproduction in any medium, provided the original work is properly cited.

© 2025 The Author(s). *Journal of Magnetic Resonance Imaging* published by Wiley Periodicals LLC on behalf of International Society for Magnetic Resonance in Medicine.

To discriminate between different tissue EPs, heterogeneous phantoms should be used. The phantom's compartments can be separated with plastic boundaries (e.g., for liquid-based compounds) or kept in direct contact (gel-based compounds). Liquid-based compounds may be suboptimal due to the risk of flow artifacts in images, which are avoided in gel-based compounds. Gel-based compounds may be put in direct contact [4], but electrolyte diffusion between compartments may alter the conductivity and internal geometry near the interfaces, as highlighted in [5–7]. To avoid these issues, solid structures can be used to separate different compartments. However, due to the significant mismatch in EP between the plastic dividers and adjacent tissue-mimicking materials, these interfaces introduce localized artifacts [1]. In particular, at least one voxel in the magnitude transmit magnetic field is consistently corrupted by noise near the boundary. Figure 1 illustrates this boundary effect in a two-compartment cylindrical phantom, demonstrating how these image artifacts around the plastic dividers limit EP mapping assessment in small structures. Precise quantification of EP reconstruction errors related to plastic boundary thickness and material composition has not yet been established in MR-EPT literature.

2 | Phantom Composition

Phantoms should use deionized water as the solvent. Sodium chloride (NaCl) can be added to raise conductivity [5, 9–11]. Permittivity can be reduced using low-permittivity materials such as polyvinylpyrrolidone (PVP) and sucrose. Although more costly, PVP is preferred, as sucrose can lead to stability issues over time, degradation in highly concentrated solutions, caramelization when exposed to high temperatures, and T_2* shortening that may lower the SNR [12]. Ethanol and other organic solvents can also be used for permittivity reduction, but they have either poor water solubility, are volatile, or require light-proof containers [5]. Glycerol can also be used, but it can induce chemical shift artifacts [11] and its high viscosity limits its useful concentration to around 30% and 50% for gel-based and liquid-based phantoms, respectively. Barium titanate ($BaTiO_3$) or calcium titanate ($CaTiO_3$) can increase permittivity, and due to their low solubility, osmosis is negligible. $BaTiO_3$ is often preferred since it requires a lower concentration to achieve the desired permittivity value [13]. Agar or gelatin can be utilized for phantoms that require low heat diffusivity (to assess RF coil safety). Preservatives such as $CuSO_4$, Proclin, or benzoic acid can enhance stability over time. Toxic and reactive preservatives like sodium azide should be avoided.

Relaxation times, particularly T_1, can be adjusted with paramagnetic salts such as gadolinium chloride ($GdCl_3$), copper(II) sulfate ($CuSO_4$), or manganese(II) chloride ($MnCl_2$) [14]. $GdCl_3$ requires a lower concentration as a T_1-shortening agent [14], which helps minimize diffusion effects in phantoms without plastic boundaries, but it is toxic and has a pronounced impact on EP due to its high ionic charge. Agar and gelatin can also be used as T_1 and T_2 shortening agents [1, 11, 14, 15].

Phantom components should be weighed before construction to minimize errors in concentrations and potential mass loss during the high-temperature steps of the mixing process. Once the Larmor frequency and target EPs are established according to the organ or the tissue of interest (e.g., brain, prostate, liver, etc.), the required amounts of PVP and NaCl may be calculated using, for example, the software outlined in [12].

Realistic tissue EPs should be targeted in phantom preparations, for example, relative permittivity <120, conductivity <2.5 S/m for 3 T [1]. When the conductivity is negligible, high permittivity can lead to interfering B_1 patterns due to its inverse relationship with the wavelength, especially at fields ≥ 3 T [9]. High conductivity may give rise to B_1 inhomogeneities due to eddy currents [9], which at fields ≥ 3 T can impair the performance of EPT methods that are based on specific assumptions that may no longer hold (namely, the transceive phase assumption, or negligible B_z gradient).

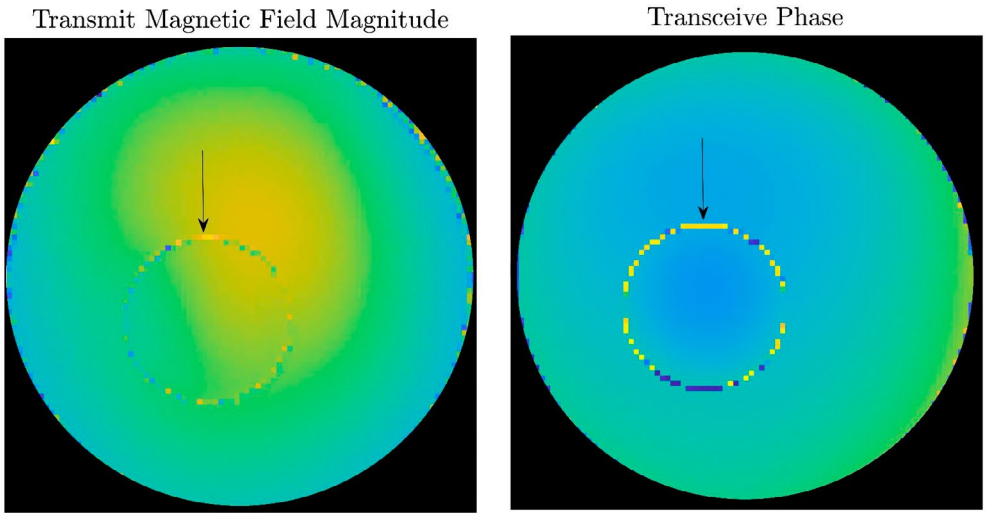

FIGURE 1 | Magnitude of the transmit magnetic field (left) and transceive phase (right) for an axial slice of a two-compartment cylindrical phantom (details on compartment EP values are provided in the next sections). The phantom was scanned at 2.5 mm isotropic resolution using the RF map sequence [8]. The plastic boundary separating the two compartments was approximately 2.5 mm thick. This boundary region is noisy due to the lack of MR signal in both the magnitude and phase maps.

15222586, 0, Downloaded from https://onlinelibrary.wiley.com/doi/10.1002/jmri.70059 by National Institute Of Standard & Technology (Nist), Wiley Online Library on [20/11/2025]. See the Terms and Conditions (https://onlinelibrary.wiley.com/terms-and-conditions) on Wiley Online Library for rules of use; OA articles are governed by the applicable Creative Commons License

3 | Example Procedure for Phantom Preparation

First, weigh the appropriate amount of water in a sealable borosilicate glass bottle. Second, dissolve the NaCl in the water. Third, gradually add the PVP (if used) while stirring vigorously. If the PVP concentration exceeds 30%, heat the solution to 60°C in a microwave oven. Typically, 500 g of solution is heated for 4 min at 900 W in a commercial microwave oven. Depending on PVP concentration, this procedure could be repeated, keeping the solution under agitation until it becomes fully transparent with a slight amber tint [16]. After this stage, agar or gelatin can be added for gel-based phantoms. The mixture should be heated up to allow them to fully dissolve (agar: > 95°C, gelatine: > 70°C). Finally, during the cooling step under agitation (at room temperature), benzoic acid (or other preservatives) and the paramagnetic salt (if used) must be added for long-term stability to prevent organic degradation and to tune the phantom relaxation times, respectively. Pouring into the phantom scaffold should be done carefully when the solution temperature is > 65°C, since the higher viscosity traps air bubbles at lower temperatures. Gentle shaking of the hot solution helps raise the bubbles to the surface. Alternatively, one can vacuum the material [17] or keep it in a water bath for 45 min before allowing it to cool to room temperature [18]. For gel-based heterogeneous phantoms, solidification of the first gel is required before pouring the next one [4]. The application of this procedure with the quantities reported in Table 1 would result in two materials (C-1 and C-2) mimicking the electromagnetic behavior of cerebrospinal fluid and gray matter when exposed to the RF field of a 3 T MRI scanner.

4 | Phantom Lifetime

A quality assurance protocol should be put in place to monitor the temporal stability of the phantom. However, since the criteria for determining when a phantom should be decommissioned are yet to be defined, reporting the lifetime of the phantom in publications can help understand the possible discrepancies between expected (from constructions) and measured EPs.

5 | Reporting

When reporting phantom recipes, all concentrations should be expressed in terms of mass/mass (g/kg, mg/g), as it is independent of temperature fluctuations. Considering the variability of EPs with Larmor frequency and temperature, we recommend reporting the target EP values for a given frequency and temperature (e.g., as calculated using [12]), and when feasible, the measured EPs with an open-ended coaxial probe [5, 19] (see an example in Table 1), including probe model. The sample characterized with the coaxial probe should be large enough to mitigate measurement errors. To improve the precision, we suggest repeating probe measurements five times and reporting the average and standard deviation values. If measurements last longer than 1 h, it is advisable to report the sample temperature before and after the experiment. If the T_1 and T_2 were modulated, it is also beneficial to report them. The type of plastic used for the phantom scaffold should also be reported. Finally, we recommend including a figure that shows the geometry and

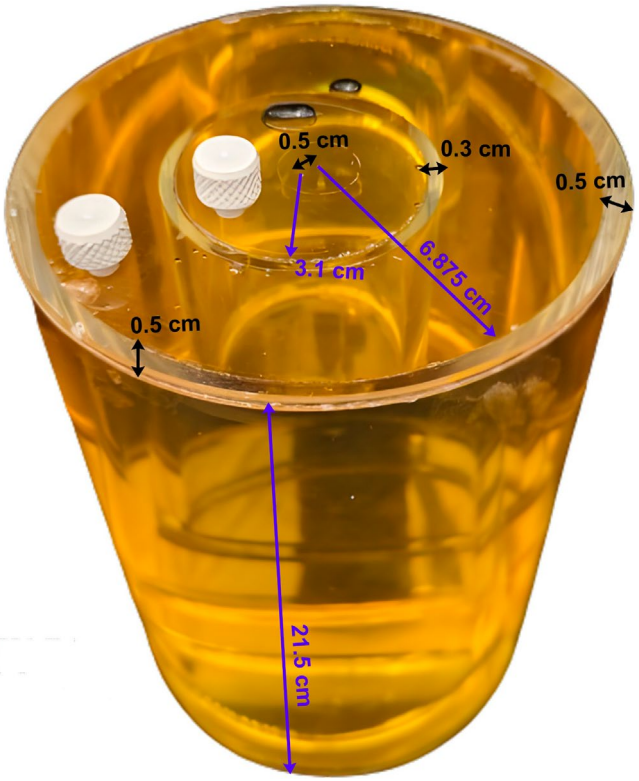

FIGURE 2 | Schematic representation of a two-compartment cylindrical liquid phantom used for EP mapping in [20]. The phantom consists of an outer hollow cylindrical and an inner cylindrical compartment. The total length of the phantom is 21.5 cm. The inner radius of the hollow cylinder is 6.875 cm, while the inner cylinder has an inner radius of 3.1 cm and is offset by 0.5 cm from the central axis of the hollow cylinder. The scaffold that contains the liquid solutions has a uniform thickness of 0.5 cm, except at the interface between the two compartments, where it is reduced to 0.3 cm.

TABLE 1 | Example recipe for a two-compartment (C-1, C-2) phantom used for EPT reconstruction at 3 T MRI.

	Recipe			Targets		Measurements			
	PVP	NaCl	$MnCl_2$	ε_r	σ_e	ε_r	σ_e	T_1	T_2
Units	g	g	mg	—	S/m	—	S/m	ms	ms
C-1	131.19	18.32	3.5	73.6	2.17	74.9 ± 3.8	1.97 ± 0.10	1080 ± 203	242 ± 12
C-2	433.96	9.41	5.3	60.9	0.60	63.8 ± 3.2	0.63 ± 0.03	875 ± 148	423 ± 8

Note: The recipe is normalized to 1 kg of water. The relative permittivity (ε_r) and the conductivity (σ_e) were measured with a dielectric probe (Agilent, Santa Clara, CA), at 22.1°C and 128 MHz. The phantom's holder was constructed using cast acrylic. T_1 and T_2 values were measured with MP2RAGE and CPMG sequences, respectively.

15222586, 0, Downloaded from https://onlinelibrary.wiley.com/doi/10.1002/jmri.70059 by National Institute Of Standard & Technology (Nist), Wiley Online Library on [20/11/2025]. See the Terms and Conditions (https://onlinelibrary.wiley.com/terms-and-conditions) on Wiley Online Library for rules of use; OA articles are governed by the applicable Creative Commons License

dimensions (compartment size and boundary thickness) to facilitate reproducibility, as in Figure 2.

Acknowledgments

I.I.G. was supported in part by National Institutes of Health K99 EB035163, and this work was performed under the rubric of the Center for Advanced Imaging Innovation and Research (CAI^{2}R, www.cai2r.net), an NIBIB National Center for Biomedical Imaging and Bioengineering (NIH P41 EB017183). A.A., T.M., A.T., L.Z. and S.M. acknowledge funding from the 24DIT01 APULEIO project. The project 24DIT01 APULEIO has received funding from the European Partnership on Metrology, co-financed from the European Union's Horizon Europe Research and Innovation Programme and by the Participating States. J.A.M. would like to acknowledge support from NIST-PREP (Professional Research Experience Program), performed under the following financial assistance award 70NANB18H006 from the U.S. Department of Commerce, National Institute of Standards and Technology. S.M. received funding from the NWO VENI Grant 18078. The following members of the ISMRM-EMTP Study Group explicitly recommend this guideline: C. Rae, Y.Z. Ider, K.K. Tha, K. Shmueli, U. Katscher, R. Dadarwal, X. Li. We also thank the whole ISMRM-EMTP study group for reviewing both the original and the revised version of the guideline.

Disclosure

Certain commercial equipment, instruments, software, or materials are identified in this paper in order to specify the experimental procedure adequately. Such identification is not intended to imply recommendation or endorsement by NIST, nor is it intended to imply that the materials or equipment identified are necessarily the best available for the purpose.

References

1. T. G. Meerbothe, S. Floczak, C. A. T. van den Berg, R. Levato, and S. Mandija, "A Reusable 3D Printed Brain-Like Phantom for Benchmarking Electrical Properties Tomography Reconstructions," *Magnetic Resonance in Medicine* 92 (2024): 2271–2279.

2. N. Westhoff, F. P. Siegel, D. Hausmann, et al., "Precision of MRI/Ultrasound-Fusion Biopsy in Prostate Cancer Diagnosis: An Ex Vivo Comparison of Alternative Biopsy Techniques on Prostate Phantoms," *World Journal of Urology* 35 (2017): 1015–1022.

3. D. Hoffmans, N. Niebuhr, O. Bohoudi, A. Pfaffenberger, and M. Palacios, "An End-To-End Test for MR-Guided Online Adaptive Radiotherapy," *Physics in Medicine and Biology* 65, no. 12 (2020): 125012.

4. L. Zilberti, A. Arduino, U. Zanovello, et al., "Magnetic Resonance-Based Electric Properties Tomography via Green's Integral Identity," *IEEE Access* 13 (2025): 42029–42044.

5. Z. He, P. M. Lefebvre, P. Soullié, et al., "Phantom Evaluation of Electrical Conductivity Mapping by MRI: Comparison to Vector Network Analyzer Measurements and Spatial Resolution Assessment," *Magnetic Resonance in Medicine* 91, no. 6 (2024): 2374–2390.

6. E. Fieremans and H. H. Lee, "Physical and Numerical Phantoms for the Validation of Brain Microstructural MRI: A Cookbook," *NeuroImage* 182 (2018): 39–61.

7. M. J. Hamamura, L. T. Muftuler, O. Birgul, and O. Nalcioglu, "Measurement of Ion Diffusion Using Magnetic Resonance Electrical Impedance Tomography," *Physics in Medicine and Biology* 51, no. 11 (2006): 2753–2762.

8. S. Akoka, F. Florence, F. Seguin, and A. Le Pape, "Radiofrequency Map of an NMR Coil by Imaging," *Magnetic Resonance Imaging* 11 (1993): 437–441.

9. M. V. Vaidya, C. M. Collins, D. K. Sodickson, R. Brown, G. C. Wiggins, and R. Lattanzi, "Dependence of and Field Patterns of Surface Coils on the Electrical Properties of the Sample and the MR Operating Frequency," *Concepts in Magnetic Resonance Part B: Magnetic Resonance Engineering* 46, no. 1 (2016): 25–40.

10. A. Stogryn, "Equations for Calculating the Dielectric Constant of Saline Water," *IEEE Transactions on Microwave Theory and Techniques* 19, no. 8 (1971): 733–736.

11. H. Yusuff, S. Chatelin, and J.-P. Dillenseger, "Narrative Review of Tissue-Mimicking Materials for MRI Phantoms: Composition, Fabrication, and Relaxation Properties," *Radiography* 30, no. 6 (2024): 1655–1668.

12. C. Ianniello, J. A. de Zwart, Q. I. Duan, et al., "Synthesized Tissue-Equivalent Dielectric Phantoms Using Salt and Polyvinylpyrrolidone Solutions," *Magnetic Resonance in Medicine* 80, no. 1 (2018): 413–419.

13. M. V. Vaidya, C. M. Deniz, C. M. Collins, D. K. Sodickson, and R. Lattanzi, "Manipulating Transmit and Receive Sensitivities of Radiofrequency Surface Coils Using Shielded and Unshielded High-Permittivity Materials," *Magma* 31 (2018): 355–366.

14. A. Antoniou and D. Christakis, "MR Relaxation Properties of Tissue-Mimicking Phantoms," *Ultrasonics* 119 (2022): 106600.

15. K. Hattori, Y. Ikemoto, W. Takao, et al., "Development of MRI Phantom Equivalent to Human Tissues for 3.0-T MRI," *Medical Physics* 40, no. 3 (2013): 032303.

16. P. Nobre, G. Gaborit, A. Troia, U. Zanovello, L. Duvillaret, and O. Beuf, "Electric Field Measurements in Preclinical MRI at 11.7 T and 7 T for Experimental SAR Comparison," *Journal of Magnetism and Magnetic Materials* 593 (2024): 171818.

17. L. Hacker, A. M. Ivory, J. Joseph, et al., "A Stable Phantom Material for Optical and Acoustic Imaging," *Journal of Visualized Experiments* 196 (2023): e65475.

18. N. P. Jerome, M. V. Papoutsaki, M. R. Orton, et al., "Development of a Temperature-Controlled Phantom for Magnetic Resonance Quality Assurance of Diffusion, Dynamic, and Relaxometry Measurements," *MedPhys* 43, no. 6 (2016): 2998–3007.

19. A. La Gioia, E. R. Porter, I. Merunka, et al., "Open-Ended Coaxial Probe Technique for Dielectric Measurement of Biological Tissues: Challenges and Common Practices," *Diagnostics* 8, no. 2 (2018): 40.

20. I. I. Giannakopoulos, G. Carluccio, M. B. Keerthivasan, et al., "MR Electrical Properties Mapping Using Vision Transformers and Canny Edge Detectors," *Magnetic Resonance in Medicine* 93, no. 3 (2025): 1117–1131.

15222586, 0, Downloaded from https://onlinelibrary.wiley.com/doi/10.1002/jmri.70059 by National Institute Of Standard & Technology (Nist), Wiley Online Library on [20/11/2025]. See the Terms and Conditions (https://onlinelibrary.wiley.com/terms-and-conditions) on Wiley Online Library for rules of use; OA articles are governed by the applicable Creative Commons License